Mon. Not. R. Astron. Soc. **000**, 000–000 (0000) Printed 17 November 2015 (MN LATEX style file v2.2)

Stellar streams around the Magellanic Clouds

Vasily Belokurov[1⋆] and Sergey E. Koposov[1]†
[1]*Institute of Astronomy, Madingley Rd, Cambridge, CB3 0HA*

17 November 2015

arXiv:1511.03667v2 [astro-ph.GA] 16 Nov 2015

ABSTRACT
Using Blue Horizontal Branch stars identified in the Dark Energy Survey Year 1 data, we report the detection of an extended and lumpy stellar debris distribution around the Magellanic Clouds. At the heliocentric distance of the Clouds, overdensities of BHBs are seen to reach at least to $\sim 30^\circ$, and perhaps as far as $\sim 50^\circ$ from the LMC. In 3D, the stellar halo is traceable to between 25 and 50 kpc from the LMC. We catalogue the most significant of the stellar sub-structures revealed, and announce the discovery of a number of narrow streams and diffuse debris clouds. Two narrow streams appear approximately aligned with the Magellanic Clouds' proper motion. Moreover, one of these overlaps with the gaseous Magellanic Stream on the sky. Curiously, two diffuse BHB agglomerations seem coincident with several of the recently discovered DES satellites. Given the enormous size and the conspicuous lumpiness of the LMC's stellar halo, we speculate that the dwarf could easily have been more massive than previously had been assumed.

Key words: Galaxy: fundamental parameters — Galaxy: halo — Galaxy: kinematics and dynamics — stars: blue stragglers — stars: horizontal branch

1 INTRODUCTION

This Universe is conjectured to have assembled hierarchically, from the bottom up, yet the evidence for accretion onto dwarf galaxies with luminosities $\leqslant 10^{10} L_\odot$ is currently scarce (Rich et al. 2012; Martínez-Delgado et al. 2012; Amorisco et al. 2014). In the cosmic pecking order, the Magellanic Clouds are just a position down from the Milky Way and, hence could, in principle, given their proximity, serve as a typical example of the sub-L_* satellite galaxy assembly in the ΛCDM Cosmology. The extent and the amount of lumpiness in the stellar halo (if it exists) of the Large Magellanic Cloud (LMC) would not only present another crucial piece of evidence that our structure formation theory works on all scales; it would also give us a close-up view of the emergence and the destruction of sub-structure within sub-structure. Moreover, the LMC's dark matter (DM) distribution as well as the galaxy's orbital history could be accurately constrained. However, to date, the details of the gravitational interaction between the LMC and the SMC remain muddled, and precious little information is available as to the signs of accretion of even smaller fragments onto either of the Clouds.

The gravitational interaction between the two Clouds has been under a close scrutiny ever since the Magellanic gaseous Stream (MS) was discovered (Wannier & Wrixon 1972; Mathewson et al. 1974). First attempts at modelling the MS inaugurated a new promising sub-field of Galactic Astronomy, the Stream Dynamics, yielding new interesting constraints on the DM halo of the Milky Way (e.g. Davies & Wright 1977; Lin & Lynden-Bell 1977; Lin et al. 1995) as well as its gaseous halo (Meurer et al. 1985; Moore & Davis 1994; Heller & Rohlfs 1994; Mastropietro et al. 2005) depending on the mechanism assumed responsible for the production of the Stream. Very quickly it was established that the Stream ought to originate from the SMC rather then the LMC (Murai & Fujimoto 1980; Connors et al. 2006), thus bringing into light the complex history of three-body encounters between the Clouds and the Galaxy. Even though the time the Clouds have spent together is not well constrained, several MS simulations revealed that it was possible for the LMC and the SMC to become a pair only recently as most of the salient MS features could be reproduced with a 2 Gyr orbital history (e.g. Gardiner & Noguchi 1996). As the observational data on the gas in the MS and the Clouds themselves grew in volume and complexity (Putman et al. 2003; Harris & Zaritsky 2006; Kallivayalil et al. 2006a,b; Nidever et al. 2008, 2010; Kallivayalil et al. 2013), so did the numerical models (Besla et al. 2007, 2010; Diaz & Bekki 2011, 2012).

As every tidal model of the MS production predicts a stellar counterpart to the observed gaseous component, several searches were conducted to uncover stars coincident with the Stream (Sanduleak 1980; Recillas-Cruz 1982; Brueck & Hawkins 1983; McMahon & Irwin 1989; Kunkel et al. 1997; Guhathakurta & Reitzel 1998). Intriguingly, none of them yielded a convincing detection. The null detection could either be viewed as an argument against the tidal nature of the MS, or explained by the extremely low surface brightness levels of the stellar debris, actually in agreement with most simulations (Weinberg 2000; Diaz & Bekki 2012; Besla et al. 2013). Additionally, as Diaz & Bekki (2012) argue, the gaseous stream produced

⋆ E-mail:vasily@ast.cam.ac.uk
† E-mail:koposov@ast.cam.ac.uk

© 0000 RAS

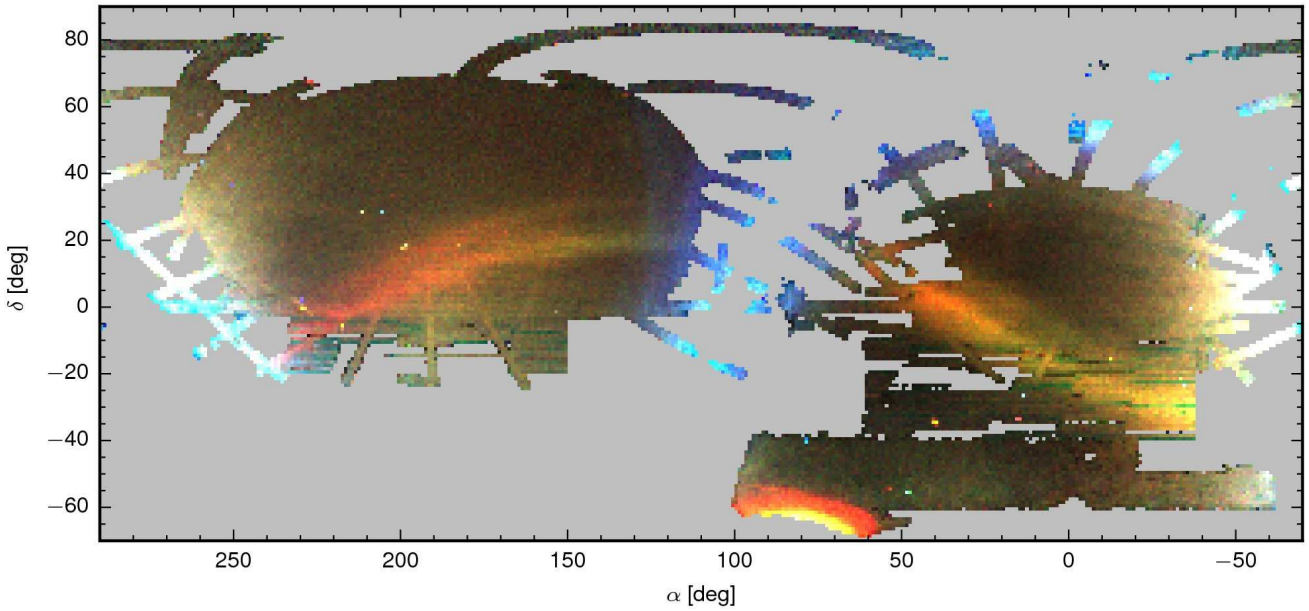

Figure 1. Jigsaw puzzle of the Galactic stellar halo as traced by the MSTO stars. This false-colour composite image combines data from three different surveys: SDSS DR9, VST ATLAS and DES Year 1. R, G and B channels of the image are greyscale density maps of stars with $0.2 < (g-i) < 0.5$ within the following magnitude ranges: $22 > i > 21$ (red), $21 > i > 20$ (green) and $20 > i > 19$ (blue). The Sgr stellar stream and the LMC (with the centre at $\alpha = 80\overset{\circ}{.}9$ and $\delta = -69\overset{\circ}{.}7$) are the most prominent halo structures visible. Note also two faint and fuzzy overdensities of approximately green colour at RA$\sim 100^\circ$ and RA$\sim 30^\circ$. These must lie much closer along the line of sight as compared to the LMC.

by stripping of the disk and the stellar stream originating (at least in part) from the SMC's old spheroid could be misaligned.

Seemingly more successful have been the attempts to map out the stellar halo of the LMC. Bits of the evidence in favour of an extended spheroidal component come from the kinematics of planetary nebulae and RR Lyrae (e.g. Feast 1968; Minniti et al. 2003). On the other hand, globular clusters have been shown not to be part of a halo (Freeman et al. 1983). Star count maps built with a variety of tracers have helped to detect shreds of an extended structure beyond 10° (and as far as 15 kpc) from the LMC (e.g. Irwin 1991; Kinman et al. 1991). However, according to Alves (2004), these measurements are also consistent with an extended disk model. Several studies have gone as far as $\sim 20^\circ$ from the Cloud. For example, Majewski et al. (1999, 2009) report a kinematic detection of the LMC red giant branch (RGB) stars at around 23°. Similarly, Muñoz et al. (2006) traces RGB stars consistent with the origin in the LMC to the location of the Carina dwarf, i.e. 22° from the LMC. This detection is confirmed by McMonigal et al. (2014) with the help of a matched filter technique applied to the deep follow-up imaging around Carina. Unfortunately, yet again, as shown most recently by Mackey et al. (2015), rather than a genuine halo population, these stellar debris could be a part of the large stream-like feature that appears to be torn off the LMC's disk.

Perhaps the most comprehensive approach to date to surveying the periphery of the Magellanic System is exemplified by the Outer Limits Survey (Saha et al. 2010), which gathered deep multi-band photometry over tens of square degrees around the Clouds. The OLS reports unambiguous identification of LMC's Main Sequence stars out to 16° (from the LMC). Moreover, the star counts appear to follow an exponential profile. As the authors point out, the most straightforward interpretation of this result is that the LMC's disk stretches as far as 10 scale lengths. However, according to Saha et al. (2010), if the mixture of the LMC's structural components looked anything like that of the Milky Way, the disk would anyway dominate the star counts to at least 10 scale lengths, or further. Therefore, even though the OLS does not detect the LMC's stellar halo, it can not confirm its absence either.

As illustrated above, the quest to track down stellar debris at large distances from the LMC (and the SMC) appears to have been frustrated by the lack of deep, wide and *continuous* coverage of the outskirts of the Magellanic Clouds. Motivated by this, we choose to scout for the Magellanic stellar halo sub-structure using Blue Horizontal Branch stars selected from the Dark Energy Survey (DES) Year 1 public dataset. First, the DES delivers an uninterrupted view of the relevant patch of the Southern sky that is an order of magnitude larger in area compared to all previous surveys, while reaching depths similar to the most ambitious of the earlier attempts. The choice of BHBs as tracers is rather obvious too: these old and metal-poor stars suffer little contamination from other stellar populations, can be easily picked up as far as 100 kpc or beyond, and, finally, are one of the best stellar standard rulers available. This paper is organised as follows. To begin with, we present a panoramic view of the Milky Way stellar halo in Section 2. This is followed by presentation of the details of the BHB selection process in Section 3. We describe the sub-structure uncovered in Section 4. Finally, Section 5 summarizes our discoveries and puts them into context.

2 THE BIGGER PICTURE. THE GALAXY'S STELLAR HALO

The Magellanic Clouds are on their way to merge with the already crowded Milky Way halo. To place the subsequent analysis into perspective, we create a mosaic map of the Galactic stellar halo

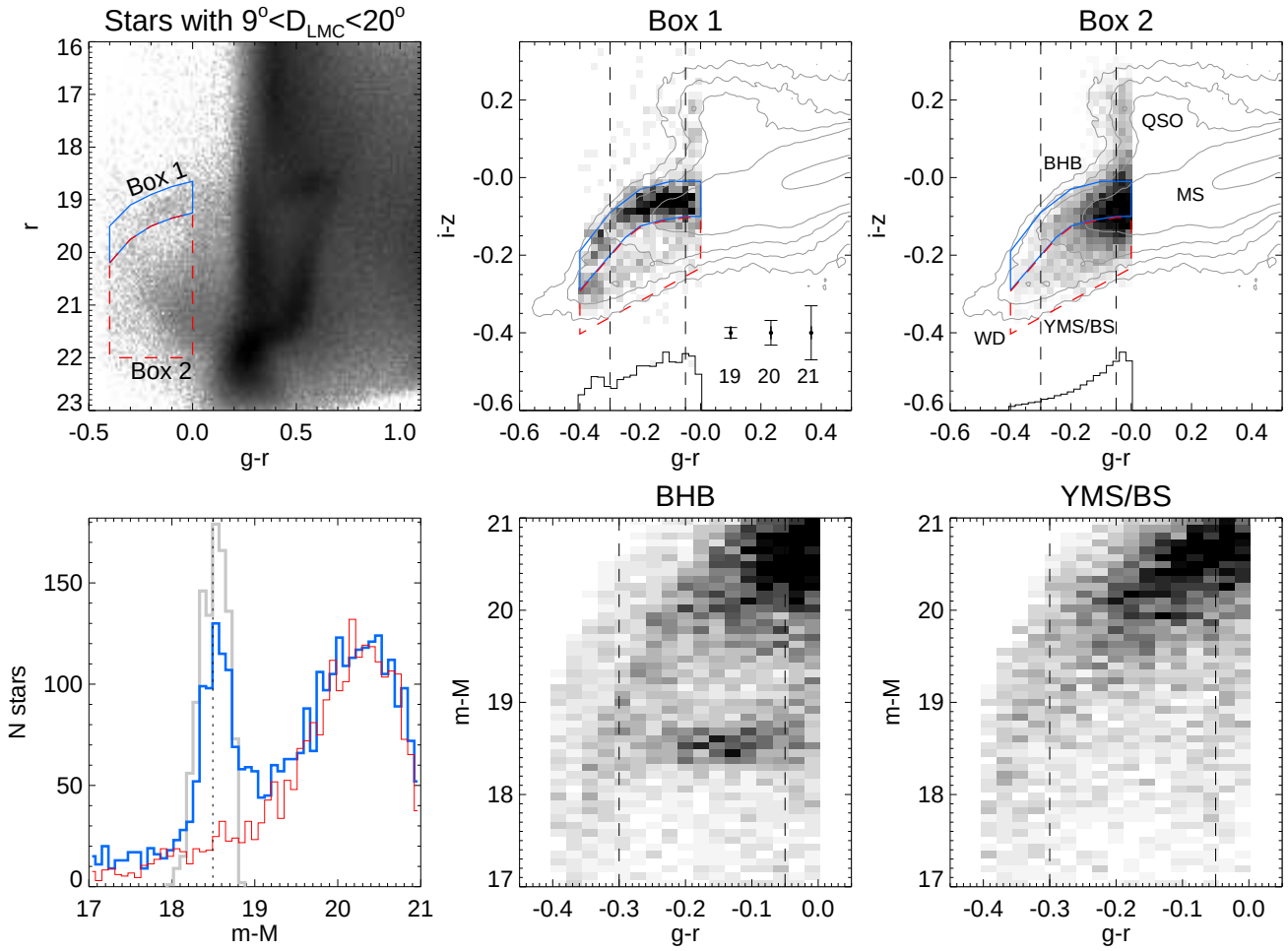

Figure 2. Blue Horizontal Branch star identification with the DES's $griz$. *Top left:* Hess diagram (CMD density) of all stars with $9^\circ < D_{\rm LMC} < 20^\circ$. Familiar features such as the Main Sequence Turn-Off, the Red Giant Branch and the Red Clump are visible in the red portion of the CMD ($g-r>0$). In the blue, two features stand out: the Blue Horizontal Branch (at $r<20$) and the cloud of Young Main Sequence and Blue Straggler stars (with $r>20$). Blue (red) lines mark the selection Box 1 (Box 2) used to isolate the BHB (YMS/BS) stars. *Top centre:* Density in the $g-r, i-z$ plane for stars selected to lie in the Box 1 in the top left panel. Contours give the density distribution of all stars. A tight sequence of genuine BHB stars is visible, curving from $g-r\sim 0$, $i-z\sim -0.1$ to $g-r\sim -0.4$, $i-z\sim -0.3$. Blue (red) box shows the colour-colour decision boundary used to select BHB (YMS/BS) stars. The coordinates of the vertices of the selection boxes are given in Tables 1 and 2. Vertical dashed lines show the restricted range of $g-r$ used for the BHB selection reported here. The histogram gives the $g-r$ distribution of the BHB stars that passed both the CMD and colour-colour cuts. Three points with error-bar demonstrate the behaviour of $i-z$ error as a function of r for stars with $g-r<0$ and $i-z<0$. *Top right:* Same as the top centre panel, but for the stars in Box 2. Portions of the $g-r, i-z$ space are marked with the names of objects dominating the density at that location. *Bottom left:* Distance modulus distribution. The blue (red) line gives the histogram of $m-M$ calculated using a version of equation 7 of Deason et al. (2011), for all stars with $9^\circ < D_{\rm LMC} < 20^\circ$ lying in the blue (red) box shown in the top centre and top right panels. The blue curve corresponds to the LMC's BHB stars and peaks at $m-M\sim 18.5$ in perfect agreement with the recent measurement by Pietrzyński et al. (2013). Grey line is the histogram of BHB candidate stars selected using both CMD cuts shown in top left panel as well as the colour-colour cuts shown in the center and right panels. *Bottom center:* BHB distance modulus as a function of the $g-r$ colour. Density of stars selected using the blue box from the panel directly above is shown. Notice the growing contamination from the YMS/BS stars outside the region marked with dashed lines. *Bottom right:* Same as previous panel, but for the YMS/BS stars selected using the colour-colour box shown in red.

in equatorial coordinates, shown in Figure 1. This panoramic view of the Galaxy's outskirts is put together using MSTO stars from three different surveys: SDSS DR9 (Ahn et al. 2012), VST ATLAS (Shanks et al. 2015) and DES Year 1 (Koposov et al. 2015). This false-colour composite image shows density distributions of stars with $0.2<(g-i)<0.5$ in three different magnitude ranges. The red channel corresponds to the density of MSTO stars with $21<i<22$ (most distant stars), the green channel gives the density of stars with $20<i<21$, and the blue channel corresponds to the nearest MSTO stars with $19<i<21$.

The two most prominent structures in this map are the Sagittarius stream (see e.g. Majewski et al. 2003; Belokurov et al. 2006; Koposov et al. 2012; Belokurov et al. 2014), looping through the entire sky covered by the SDSS and the VST ATLAS, and the LMC at $100^\circ > {\rm RA} > 50^\circ$ at the bottom of the DES Year 1 footprint. Even though many other familiar halo sub-structures are discernible elsewhere in the image, we limit our attention to several new overdensities visible in the area of the sky covered by the DES survey. Seemingly connected to the LMC disk at RA$\sim 100^\circ$, a faint and almost vertical tail of MSTO stars is noticeable. It is possible though that rather than being a genuine halo substructure, this overdensity is related to the disk instead, since its galactic lat-

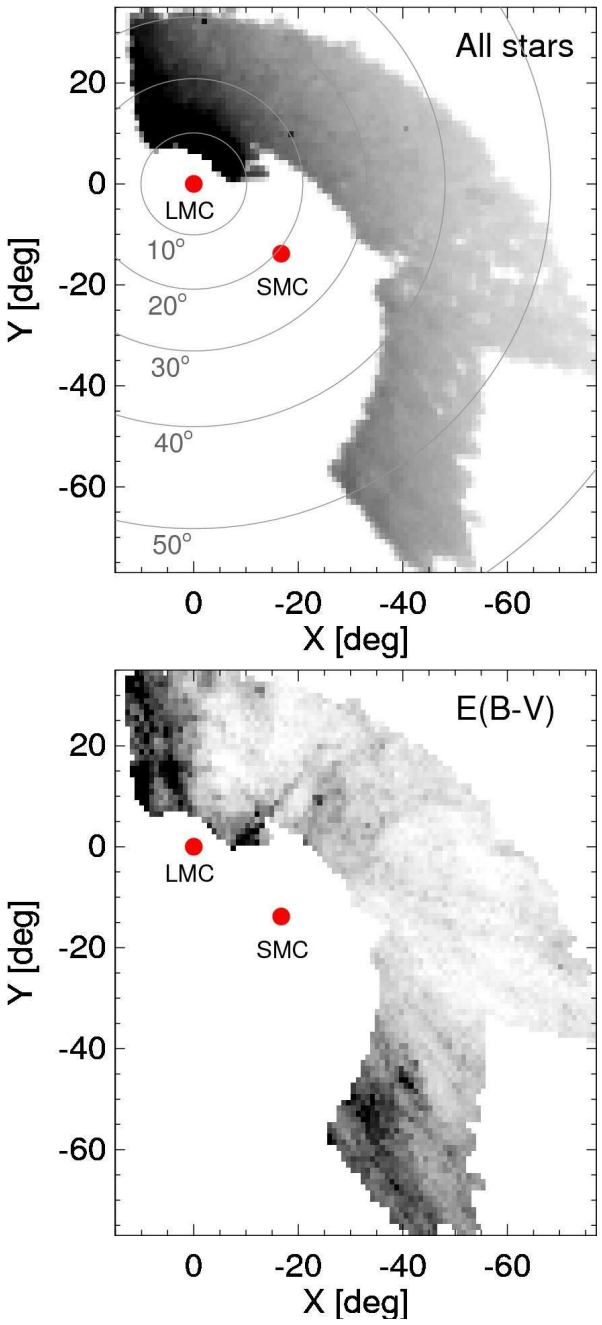

Figure 3. *Top:* Density of all stars in the DES Year 1 dataset in gnomonic projection with the tangent point at the LMC's location. Filled red circles mark the locations of the LMC and the SMC. Lines of equal spherical distance from the LMC are also shown. This map is 100 pixels on the side. *Bottom:* Distribution of the Galactic reddening in the survey's footprint. The map has the same dimensions as that shown in the left panel. The greyscale is set to vary between the 2nd and the 98th percentiles of the $E(B-V)$ values in the area, i.e. 0.0075 and 0.075.

itude is $b \sim -25^\circ$. Additionally, there is a fuzzy and faint green overdensity of stars at around RA$\sim 30^\circ$. This stellar cloud has been recently reported as Eridanus-Phoenix overdensity by Li et al. (2015).

Given their colour in Figure 1, the two DES MSTO overdensities mentioned above are located much closer along the line of sight as compared to the LMC. Their genealogy is yet unknown, but their proximity to the Magellanic Clouds might turn out to be purely coincidental. Note that apart from these two rather faint overdensities and the LMC itself, the area covered by the DES Year 1 data appears rather quiet and unremarkable, as traced by the MSTO stars. However, the BHBs tell a very different story.

3 BLUE HORIZONTAL BRANCH STAR IDENTIFICATION WITH DES

To study the stellar halo sub-structure around the Magellanic Clouds, we use the photometric catalogs obtained from the publicly released DES Year 1 imaging (see Koposov et al. 2015, for details), in particular, the latest improved version of the reduction as reported in Mackey et al. (2015). While the calibration of the gri-band data has been described in Koposov et al. (2015), the calibration of the z-band data requires a separate discussion, as it was done differently to the gri photometry. The reason is the lack of z-band measurements in the APASS (the AAVSO Photometric All-Sky Survey) catalogue. Therefore we compute the APASS z-band magnitude using the g and r APASS magnitudes. More precisely, we describe the SDSS (and therefore also APASS) z-band magnitude as a 4-th degree polynomial of the $g-r$ colour [1]. The limiting magnitude in the z band is ~ 21.9.

DES provides the deepest and widest panorama of the environs of the Magellanic Clouds to date. The survey's Year 1 footprint covers only a portion of the halo of the LMC and an even smaller segment of the SMC's outskirts. However, the DES's uninterrupted view is crucial when making sense of such a large, diffuse and fragmented structure. Our catalogs cover $\sim 2200^\circ$ square degrees just North of the Clouds and contain $griz$ magnitude measurements (tied to the SDSS/APASS photometric system) for $\sim 1.5 \times 10^8$ stars with $g < 23.5$. In the analysis that follows, the photometry is corrected for the effects of extinction using the dust maps of Schlegel et al. (1998) and the conversion suggested by Schlafly & Finkbeiner (2011). For the star/galaxy separation, we use the following conservative cut: $|\mathrm{SPREAD_MODEL}| < 0.002$ simultaneously in three bands, g, r and i. Note that at faint magnitudes, this morphological classification is less complete, but more pure as compared to the criterion used in Koposov et al. (2015).

BHBs are a go-to stellar tracer for the Galactic halo studies (see e.g. Yanny et al. 2000; Newberg et al. 2003; Xue et al. 2008; Bell et al. 2010; Ruhland et al. 2011; Deason et al. 2011). In the halo, not only can these old and metal-poor stars be easily identified above the foreground of other populations thanks to their peculiar colour, they are also one of the best stellar distance estimators available, outperformed only by their immediate neighbors on the Hertzsprung-Russell diagram, the RR Lyrae. Thanks to their unique properties, BHBs have proven to be a powerful tool to scrutinize the Galactic halo out from the core to its far-flung fringes (e.g. Belokurov et al. 2014; Deason et al. 2014).

As the name suggests, the spectral energy distribution of a BHB star peaks at short wavelengths. There, in the blue, minute changes in the shapes of the Balmer lines accumulate to provide a powerful diagnostic to distinguish BHBs from other stars with similar temperatures (see e.g. Sirko et al. 2004). Impressively, these signatures can also be picked up by means of broad-band photometry only (see e.g. Yanny et al. 2000). Provided an accurate measurement of near-UV flux excess exists, e.g. SDSS's $u-g$ colour,

[1] $z = -0.2126 + 1.2227(g-r) - 4.1545(g-r)^2 + 4.0484(g-r)^3 - 1.4355(g-r)^4$

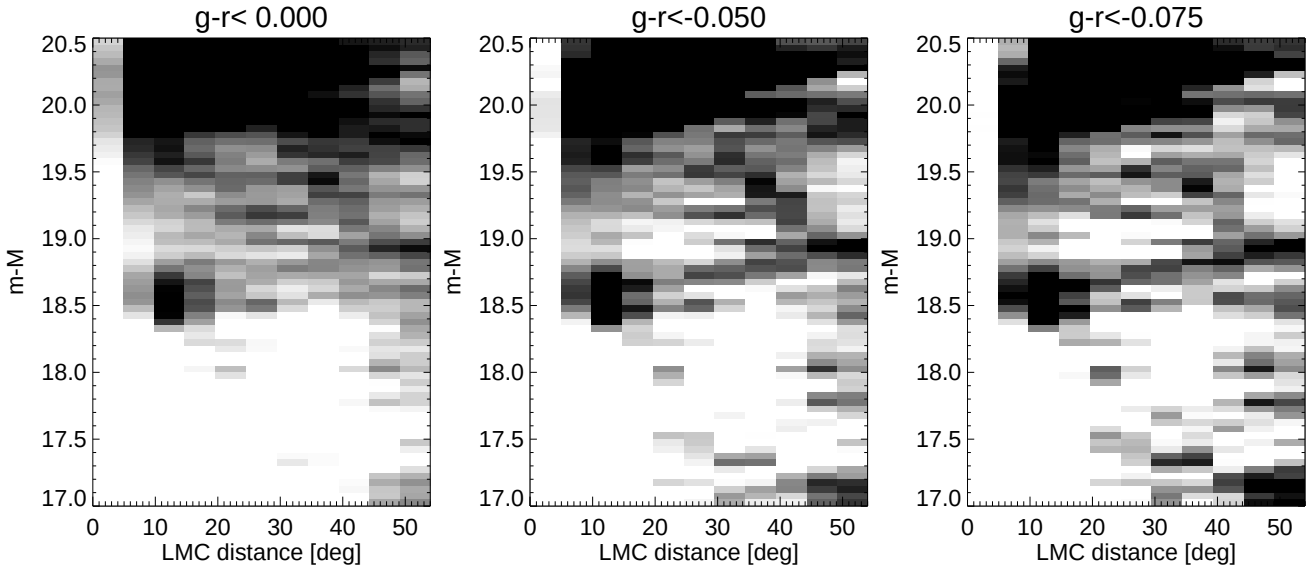

Figure 4. Stellar sub-structure around the Magellanic Clouds as traced by BHBs. Each panel shows the density of the BHB candidate stars in the plane of distance modulus and the angular distance from the LMC. The maps are 11×70 pixels, and are smoothed with a Gaussian kernel with a FWHM of 1.7 pixels. From left to right, the red $g-r$ cut used for the BHB selection (see Figure 2) is lowered from 0 to -0.075, as indicated at the top of each panel. Limiting the BHB candidate selection to bluer $g-r$ colours helps to improve the effects of the YMS/BS contamination. The contamination is most severe in the distribution shown in the left panel. As the YMS/BS contamination becomes reduced (middle panel), several dark (corresponding to an enhanced BHB density) sequences are clearly visible starting at $m-M\sim18.5$, i.e. the LMC's heliocentric distance. The signal strengths improves as the BHB sample becomes purer (right panel): the most prominent dark band corresponds to the BHB debris whose heliocentric distance increases with angular distance from the LMC. As obvious from the last two panels, the LMC's stellar halo, as traced by BHBs, extends out to $\sim50^\circ$ from the dwarf. Note that the DES coverage is very sparse near the LMC center, however, at distances larger than 10° more than a quarter of the LMC halo is sampled by DES.

BHBs immediately break away from quasars and White Dwarfs (WD). Differences between Young Main Sequence stars (YMS) or similarly looking Blue Stragglers (BS) and BHBs are more subtle and typically require higher quality u-band photometry (see e.g. Deason et al. 2012). DES, however, does not observe in the u band, hence the BHB identification techniques described above are not applicable. Nevertheless, as shown by Vickers et al. (2012), near-IR photometry can be used instead with an almost equally impressive success. According to the authors, rather than the Balmer series, the Paschen lines serve as the discriminator, resulting in the noticeable differences in the $i-z$ colour of BHBs, QSO, WDs and YMS/BS stars.

Figure 2 gives the details of the BHB selection process as applied to the DES data. Top left panel of the Figure shows the Hess diagram (i.e. the density of stars in the colour-magnitude space) of all stars with angular separations between 9° and 20° from the center of the LMC, which we assume to have coordinates $\alpha=80\overset{\circ}{.}8937$ and $\delta=-69\overset{\circ}{.}7561$ (McConnachie 2012)[2]. At these distances, the Colour-Magnitude Diagram (CMD) contains plenty of both young and old populations, most easily discernible at $g-r<0$. The selection Box 1 (Box 2) used to isolate the BHB (YMS) candidate stars are shown in blue (red) respectively. It is clear from this CMD, that even though the BHBs dominate at brighter apparent magnitudes, the YMS/BS contamination of the area shown in blue is not negligible. The greyscale density of the thus selected BHB candidates in the plane of $g-r$ and $i-z$ colours can be seen in the top middle panel of the Figure. The narrow and curving overdensity corresponding to the genuine BHBs is clearly visible. The boundaries of the BHB signature are demarcated by the box shown in blue. At bluer $i-z$ colours lie the YMS and BS stars, mixed with Galactic WDs - this region of $g-r$,$i-z$ plane is marked with a dashed red line. The coordinates of the $g-r$,$i-z$ selection boxes are given in Tables 1 and 2.

The highly clustered behaviour of the BHBs in the colour-colour space can be contrasted with the distribution of YMS/BS stars, as shown in the top right panel of Figure 2. The MS and pseudo-MS stars tend to congregate at redder $g-r$ colours and cover a much broader range of $i-z$ colour. At the bottom of each of the two panels, a histogram showing the corresponding $g-r$ distribution is given to emphasise these differences. It appears beneficial to get rid of the reddest (in $g-r$ sense) of the BHB candidates to minimise the YMS/BS contamination. Further insight into the properties of the selected BHB candidates can be gleaned from the panels in the bottom row of the Figure. Here, distributions of the distance modulus values of the BHB and YMS/BS samples are depicted, assuming the same BHB absolute magnitude calibration for both. BHB's intrinsic luminosity is primarily a function of its temperature, or equivalently, its $g-r$ colour. To this end, we use a slightly modified version of formula 7 of Deason et al. (2011) to obtain estimates of M_g and, hence, $m-M$ [3]. Note, however, that as pointed by Fermani & Schönrich (2013), the BHB's absolute magnitude also weakly depends on its metallicity.

Blue (red) histogram in the bottom left panel of Figure 2 gives

[2] Note, however, that the dynamical centre of the LMC has recently been estimated to lie at $\alpha=78\overset{\circ}{.}76$ and $\delta=-69\overset{\circ}{.}19$ by van der Marel & Kallivayalil (2014)

[3] $M_g=0.398-0.392(g-r)+2.729(g-r)^2+29.1128(g-r)^3+113.569(g-r)^4$. This absolute magnitude is only $\sim$0.02 mag brighter than that of Deason et al. (2011), and hence all results presented here should remain unchanged if their calibration is used.

Table 1. Boundaries of the BHB selection box

$g-r$	-0.4	-0.3	-0.25	-0.2	-0.13	-0.05	0.0	0.0	-0.1	-0.2	-0.3	-0.4	-0.4
$i-z$	-0.3	-0.2	-0.2	-0.1	-0.1	-0.1	-0.1	-0.0	-0.0	-0.0	-0.1	-0.2	-0.3

Table 2. Boundaries of the YMS/BS selection box

$g-r$	-0.4	-0.3	-0.25	-0.2	-0.13	-0.05	0.0	0.0	-0.4	-0.4
$i-z$	-0.3	-0.2	-0.2	-0.1	-0.1	-0.1	-0.1	-0.2	-0.4	-0.3

the distance modulus distribution for stars that fall into the blue (red) box shown in the top middle and top right panels, i.e. the BHB (YMS/BS) stars. Additionally, these are limited to lie in the same range of angular distances as the stars displayed in the top left panel, and have $-0.3 < g-r < -0.05$. At low $m-M$, the BHB distribution peaks at ~ 18.5 which is in perfect agreement with the recent LMC distance estimate by Pietrzyński et al. (2013). To illustrate the completeness of the proposed BHB selection, underlying the blue histogram, is the grey line showing the distribution of stars selected as above but instead of the $griz$ cut, required to lie in the blue box shown on the CMD in top left panel of the Figure. The difference in height between the blue and grey peaks is predominantly due to the polluting YMS/BS stars. The YMS/BS histogram, shown in red, shows no appreciable amount of BHBs around the LMC distance modulus, and peaks $\sim$2 mag further. Note that these large $m-M$ values do not correspond to the true distances to these stars, but rather reflect the fact that they are on average $\sim$2 mag fainter as compared to the BHBs. The need for the additional $g-r$ cut as mentioned above becomes clear on examination of the bottom middle panel. Here, the behaviour of the $m-M$ as a function of the $g-r$ colour is shown for the BHB candidates. Outside the $-0.3 < g-r < -0.05$ range, the BHB and YMS/BS sequences start to merge and the contamination tends to increase. Additionally, as obvious from the left panel of Figure 4 of Deason et al. (2011) and the middle panel of Figure 1 of Belokurov et al. (2014), outside this $g-r$ range, the BHB absolute magnitude can deviate mildly from the ridgeline prescribed by the polynomial fit.

Overall, as this Section demonstrates, for a particular $g-r$ range, a simple $griz$ selection box can be used to obtain highly complete samples of BHB stars. Such samples will always be contaminated with YMS/BS stars, and this contamination grows for stars with redder $g-r$ colour. However, in the distance modulus space, the contaminants' distribution always appears broader. Moreover, for co-distant populations, this contamination peaks $\sim$2 mag fainter, and as such, can be easily identified and discarded. Quite simply, there is enough evidence to conclude that the asbolute majority of narrow peaks in the $m-M$ should be attributed to the BHBs.

4 BHB OVERDENSITIES AROUND THE MAGELLANIC CLOUDS

As the DES Year 1 footprint provides a better view of the LMC's surroundings as compared to the SMC's coverage, we choose to present the maps of the BHB density distribution in a gnomonic projection centred on the LMC (similar to e.g. Mackey et al. 2015). The shape of the survey's footprint in these coordinates can be seen in Figure 3. The top panel of the Figure shows the greyscale density distribution of all stars in the dataset. The dramatic density enhancement in the left corner of the DES Year 1 field of view is partly due to the LMC's stars (at $-10^\circ < X < 10^\circ$ and $Y < 15^\circ$) and partly due to the Galactic disk (at $X \sim 10^\circ$). While the footprint shape is roughly rectangular in equatorial coordinates, it shows plenty of curvature far away from the tangent point. In gnomonic projection, the area is not strictly conserved, but suffers little distortion within 30° away from the LMC, as indicated by lines of equal angular distance. Beyond that, there is a noticeable stretch, i.e. objects appear further than they actually are. The footprint reaches only slightly closer than 10° from the LMC centre. The bottom panel of the Figure displays the distribution of the interstellar extinction in the DES Year 1 footprint. The greyscale is set to vary between the 2nd and the 98th percentile of $E(B-V)$ values in the area, namely 0.0075 and 0.075. This corresponds to 0.025 and 0.25 magnitudes of extinction in the g band, and 0.0095 and 0.095 magnitudes in the z band. The darker regions at either ends of the footprint show the largest (relative) amount of dust reddening. This is because these portions of the DES-covered area are closest to the Galactic disk.

Figure 4 illustrates how the Magellanic stellar halo reveals itself as layers of YMS/BS stars are gradually removed. Here, the density of the BHB candidate stars is shown in the plane of the distance modulus and the angular distance from the LMC. From left to right, the red $g-r$ cut, used for the BHB selection, is lowered from 0 to -0.075. As discussed above, the histograms in the top middle and top right panels of Figure 2 show that the BHBs and YMS/BS stars behave differently in this colour range. The density of BHBs is roughly constant, while the density of YMS/BS stars drops quickly towards the lower $g-r$ values. In accordance with this pattern, the YMS/BS contamination is highest in the left panel of Figure 4. There is a cloud of stars in the LMC disk at $d_{\rm LMC} \sim 10^\circ$ and $m-M \sim 18.5$. However, no other obvious overdensity is observable. In the middle and right panels, where the number of contaminants is diminished, there appears to be a clear BHB sequence stretching away from the LMC. This narrow BHB overdensity shows a positive distance gradient with angular separation from the dwarf. At around $d_{\rm LMC} \sim 50^\circ$, this dark band reaches $m-M \sim 19$, i.e. the heliocentric distance of the SMC (Graczyk et al. 2014). There are multiple other BHB overdensities beyond $m-M \sim 19$. However, given the faint magnitudes of the stars they are composed of, it is difficult to ascertain the authenticity of all structures present, especially those with $m-M > 20$. One striking conclusion that follows from the picture presented above, is the strong evidence for the extent of the stellar debris distribution as far as $\sim 50^\circ$ from the LMC.

While $g-r < -0.075$ cut delivers a purer selection of BHBs, it also reduces the number of tracers available. Given the fact that the overdensity maps in the middle and the right panels of Figure 4 are qualitatively the same, we choose to use $g-r < -0.05$ limit

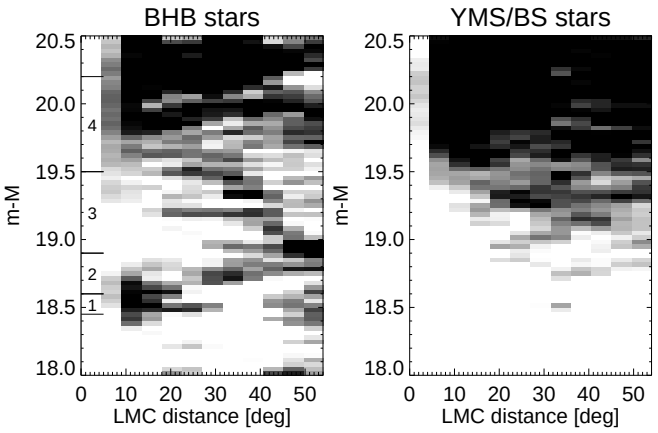

Figure 5. Line-of-sight clustering of BHBs as a function of the angular distance from the LMC. The maps are 12×75 pixels, and are smoothed with a Gaussian kernel with a FWHM of 1.7 pixels. *Left:* Density of the BHB stars in the plane of distance modulus and the distance from the LMC. As in Figure 4, several dark sequences are clearly visible starting at $m-M\sim18.5$, i.e. the LMC's heliocentric distance. Four ranges of $m-M$ explored in this work are shown on the left, and numbered from 1 to 4 for reference. *Right:* Same as the middle panel but for the YMS/BS stars. In the distance modulus ranges selected, no obvious overdensity is discernible.

as a default for the rest of the analysis. A more detailed view of the sub-structures detected is given in Figure 5. Here, left panel shows the same map of the BHB overdensities as in Figure 4, but zoomed-in onto the $m-M$ range of relevance. Curiously, in this higher resolution view, just next to the LMC, a narrow horizontal dark streak is visible, running at a constant $m-M\sim18.5$ peeling off a broader BHB sequence which slants up. This narrow sequence appears to come to an abrupt stop around $d_{\rm LMC}\sim30^\circ$. As a comparison, the right panel of the Figure presents the density of the YMS/BS stars in the same coordinates as the previous panel. While no obvious coherent patterns are visible at $m-M<20$, beyond that, the YMS/BS contamination might grow substantially high. This is due to the combination of the YMS/BS density hike and the rise of the $i-z$ error as a function of apparent magnitude (as indicated in the top middle panel of Figure 2).

To reveal the locations of individual structures around the Magellanic Clouds, the BHBs are split into four distance modulus bins (numbered from 1 to 4, as indicated in the left panel of Fig 5), namely: $18.45<m-M<18.6$, $18.6<m-M<18.9$, $18.9<m-M<19.5$ and $19.5<m-M<20.2$. The spatial distributions (in gnomonic projection, as described above) of stars in each bin are presented in Figure 6, where only the portion of the footprint nearest to the LMC is given, i.e. for stars with $Y>-20^\circ$. Each row gives three views of the sub-structure: a scatter plot of all BHBs in the corresponding distance bin, their density, and the density with auxiliary information over-plotted. It is reassuring that all structures described below are clearly visible in both scatter plots and the density distributions. Starting from the top, the first row shows the BHBs with the smallest distance modulus (corresponding to a narrow range between 49 and 53 kpc), matching that of the LMC itself. A striking, almost vertical tail of BHB stars at $X\sim0^\circ$ is visible. The structure's geometry explains the abrupt cut-off in the BHB sequence at $d_{\rm LMC}\sim30^\circ$ in the left panel of Figure 5: this is where the stream, dubbed S1, reaches the edge of the DES Year 1 footprint. Second row of the Figure shows the density of slightly more distant BHBs, i.e. those with $18.6<m-M<18.9$, corresponding to heliocentric distances between 53 and 60 kpc. Again, around the LMC, a plume of BHBs is visible, extending at least as far as $d_{\rm LMC}\sim20^\circ$. Moreover, a distinct narrow structure is clearly noticeable further out, beyond $d_{\rm LMC}=30^\circ$. This S2 stream runs diagonally from $(X,Y)=(-20^\circ,0^\circ)$ to $(X,Y)=(-45^\circ,15^\circ)$, and appears, in fact, closer to the SMC than the LMC. In the part of the sky covered by the DES Year 1 data, the stream's path follows the great circle with the pole at $(\alpha,\delta)=(298\overset{\circ}{.}5,177^\circ)$, as indicated by a red line. The third (second from the bottom) row exhibits the yet narrower and longer stream S3, traced by the BHBs with distances between 60 and 80 kpc. A great circle with the pole at $(\alpha,\delta)=(250\overset{\circ}{.}15,152\overset{\circ}{.}35)$ seems to describe this stream well (see red line in the right panel). Finally, the bottom row shows BHB candidates that are possibly located as far as 110 kpc. Here, a curving tail of stars emanating from the LMC and reaching as far as $Y\sim22^\circ$ is discernible. Additionally, a cloud of stars (dubbed S4) with $-30^\circ<X<-20^\circ$ and $0^\circ<Y<20^\circ$ can be clearly seen. Curiously, as indicated in the right panel of the row, some of the recently discovered DES satellites appear coincident with the cloud.

Also displayed in the right panel of Figure 6 are arrows representing the proper motion vectors of each of the Clouds. These are the measurements of Kallivayalil et al. (2013), corrected for the Solar reflex motion using the Sun's velocity components with respect to the local standard of rest (LSR) from Schönrich et al. (2010) and assuming $V_{\rm LSR}=235$ km s^{-1}. Additionally, blue contours show the HI density distribution in the Magellanic Stream as reported by Nidever et al. (2008). Of the several stellar debris structures described above, only the S3 stream runs parallel to the Clouds' motion and overlaps sufficiently with the gaseous stream.

Figure 7 displays the distribution of the BHB density in more familiar (yet more distorted) equatorial coordinates. Here, it is possible to show the entire DES Year 1 footprint thanks to its simple geometry in RA and Dec. The four vertically arranged panels once again correspond to the 4 distance modulus bins under consideration. Starting from the top, bins 1, 2 and 4 show clear signs of stellar sub-structure directly above the LMC, the most prominent being the S1 stream. Structures S2, S3 and S4 all show up in the corresponding maps; however, additionally, there are hints of stellar debris further away from the Magellanic Clouds, i.e. at RA$=-10^\circ$ and RA$=-50^\circ$. Given that both of these additional structures are most prominent in the density map corresponding to the distance modulus 2, they are dubbed S2a and S2b. Similar to Figure 6, approximate great circles are shown for streams S2 and S3. Positions of DES Year 1 satellites and the previously known Milky Way companions with distances less than 400 kpc are also marked with filled triangles and circles correspondingly. As noted earlier, Hor 1 and 2, as well as Eri 3 appear to be coincident with the S4 debris cloud. Moreover, in the equatorial view, the juxtaposition of Pho 2, Gru and Tuc 2 with the S2a cloud appears plausible.

4.1 Line-of-sight tomography of the debris

The most visible feature in all panels of both Figure 6 and Figure 7 is the strong overdensity of stars at the LMC's location. However, as evident from Figure 4, it is likely that amongst these, only stars with $m-M<19$ are genuine BHBs. The seemingly more distant objects are probably intrinsically fainter stars (YMS/BS) in the LMC's disk. Luckily, as discussed at the end of Section 3, it is possible to distinguish between the YMS/BS and BHB populations based on their clustering along the line of sight. Thus Figure 8 sheds light on the line-of-sight behaviour of the newly discovered

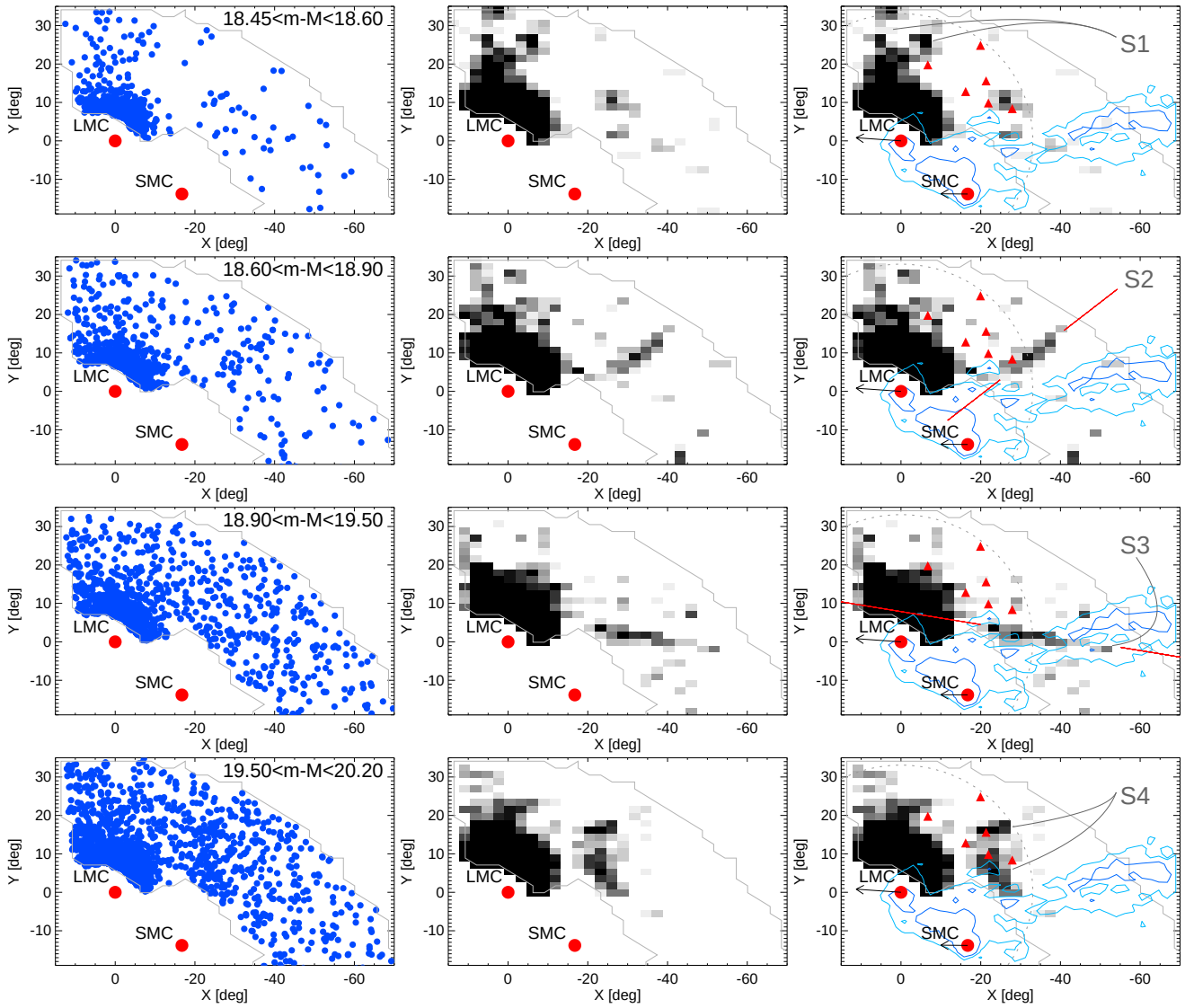

Figure 6. Distance slices of the LMC stellar halo. *Left column:* Positions of the BHB stars in four distance modulus bins marked in the Figure 5 and in the top right corner of the panel. *Middle column:* Density of the BHB stars shown in the left column. The maps are 30×30 pixels, and are smoothed with a Gaussian kernel with a FWHM of 1.5 pixels. *Right column:* As the middle column, but with auxiliary information over-plotted; this includes positions of the DES Year 1 satellites (red triangles) as well as the locations and the designations of the newly detected structures. *1st row, from the top:* This is a narrow distance range centered around the LMC's $m - M = 18.5$. A nearly vertical spray of BHB stars originating in the LMC is clearly visible, reaching all the way to the DES Year 1 footprint edge (marked with a light grey line), at $Y \sim 35°$. This sub-structure, dubbed S1, is also readily detectable in the density plots in the middle and the right panels. *2nd row:* In this distance range, stopping short of the distance of the SMC, a messy plume of BHB stars is visible directly above the LMC, stretching out as far as $Y \sim 20°$, or perhaps even beyond. Additionally, between $X \sim -40°$ and $X \sim -20°$ a narrow stream-like structure is visible crossing the footprint edge to edge. This S2 stream is well fit by a great circle with the pole at $(\alpha, \delta) = (298.^{\circ}5, 177°)$, as indicated by the red lines shown in the right panel. *3rd row:* As evidenced from the densely populated left panel, the background contamination with YMS/BS and WD stars, as well as the QSO has increased noticeably at this magnitudes. As well as the sub-structure in the northern region of the LMC's halo (as seen in the previous two distance bins), a cold nearly horizontal stream can be seen running from $X \sim -20°$ to $X \sim -60°$. The stream, dubbed S3, is approximate with the great circle with the pole at $(\alpha, \delta) = (250.^{\circ}15, 152.^{\circ}35)$. *4th row:* At these magnitudes, the background is the most severe, nonetheless, some interesting structures are still discernible. As confirmed by the density distribution, the two most prominent overdensities are i) a hook-like structures at $X \sim 0°$, $Y \sim 20°$ and ii) the S4 cloud of stars at $X \sim 35°$. on the sky, the S4 cloud appears to overlap several newly discovered DES satellites (red triangles). Arrows show the proper motion vectors of the LMC and the SMC, as measured by Kallivayalil et al. (2013) and corrected for the Solar reflex. Blue contours are the HI density of the Magellanic Stream as reported by Nidever et al. (2008). Positions on the sky with $D_{\rm LMC} = 30°$ are shown with grey dotted line.

stellar sub-structures. In particular, panels in the top row of the Figure give the greyscale BHB density maps in the plane of distance modulus and one of the pair of the X, Y coordinates (depending on the portion of the sky under consideration). For example, top left panel shows the distribution of the BHBs with $-10° < X < 5°$, i.e. those located in the patch of the sky crossing the DES Year 1 footprint vertically around the position of the LMC. A thick and mildly inclined slab of BHBs with $0° < Y < 15°$ and centered around $m - M \sim 18.5$ is presumably the disk of the LMC. At larger $m - M$, the disk BHBs are shadowed by the YMS/BS

stars. The density map is normalised vertically, i.e. each column is scaled by the total number of stars it contains. This leads to a pronounced underdensity at $m - M < 18.5$. There is also a noticeable gradient in the distribution of the YMS/BS stars, vaguely reminiscent of the letter V. Some of this pattern may be explained by the choice of the density normalisation, but the principle cause of such an appearance must be the gradient in the YMS/BS populations across the disk of the LMC. The V-shape is more obvious in the next (top middle) panel of the Figure, which presents the BHBs with $4^\circ < Y < 17^\circ$, where the V's cusp can be seen pointing at $X = 0^\circ$. The simplest interpretation of such an apparent magnitude behaviour would be the age gradient in the disk, with the younger and hence intrinsically brighter MS stars located closer to the centre.

Also visible in the top left panel of Figure 8, a much thinner strip of BHBs at a similar distance (i.e. $m - M \sim 18.5$) but extending beyond $Y \sim 14^\circ$ and reaching the edge of the footprint at $Y \sim 30^\circ$ - this is the S1 stream. The line-of-sight distribution of the BHBs in S1 does not show any obvious gradients in distance modulus as a function of Y. The bottom left panel of the Figure displays the collapsed distribution of stars in the stream, i.e. the BHBs with $-10^\circ < X < 5^\circ$ and $18^\circ < Y < 30^\circ$. There is an obvious narrow peak in the histogram with the maximum at $m - M = 18.5$. Similarly, the two middle panels present the results of the BHB tomography but for a patch of the sky with $4^\circ < Y < 17^\circ$, i.e. a horizontal slice through the LMC. As mentioned above, the LMC disk is apparent around $m - M = 18.5$ and $-10^\circ < Y < 10^\circ$. The S2 stream is visible in the top middle panel at $27^\circ < X < 40^\circ$. It does not connect to the LMC's disk feature and runs at a slightly higher distance modulus, which is supported by the histogram in the bottom middle panel, where the peak of the BHB count is $m - M = 18.75$. Finally, the top right panel presents the density of the BHBs with $-2^\circ < Y < 4^\circ$. The S3 stream can be seen as a narrow dark streak running across the entire figure from $X = -21^\circ$ to $X = -50^\circ$. According to the corresponding bottom panel, the peak distance modulus of S3 is at $m - M = 19.5$. For every structure discussed above, the significance of the BHB overdensity along the line of sight is given in the top left corner of the bottom row panels of Figure 8. We have also examined similar distance modulus slices for the structures S4, S2a and S2b. While there are peaks at around $m - M \sim 18.8$ for S2a and S2b, these are not as statistically significant as those for S1, S2 and S3 discussed above. Additionally, no obvious narrow peak is detected for S4; in fact, S4 could plausibly be produced by the overdensity of YMS/BS stars at distances similar to that of the LMC.

4.2 Notes on individual structures

In the absence of kinematical and chemical information, it is difficult to pinpoint the origin of the structures detected. Nonetheless, below, we hazard a guess based on the shape and the orientation of the debris distributions on the sky. We found our speculation on the fact that the width of the stellar stream reflects primarily the mass of its progenitor, and even though it is also a function of the stream's dynamical age as well as the asphericity of the host gravitational potential, these effects are secondary (see e.g. Johnston 1998; Erkal et al. 2015). For example, in the Milky Way, globular cluster streams are only ∼100 pc accross (see e.g. Odenkirchen et al. 2003; Grillmair & Dionatos 2006; Koposov et al. 2014), while those originating in dwarf galaxies have more substantial widths of several kpc (see e.g. Belokurov et al. 2007; Koposov et al. 2012). On the other hand, stellar streams produced as a result of the interaction between the LMC and the SMC show a variety of cross-sections, from ∼2 to 10-15 kpc (see Besla et al. 2013; Diaz & Bekki 2012), but never appear to be much narrower than 1 kpc.

4.2.1 S1 debris, LMC's stellar halo and the S4a candidate stream

Figure 9 zooms in onto the stellar debris in the immediate vicinity of the LMC. The four panels of the Figure correspond to the four distance modulus bins introduced above. Remarkably, there is plenty of evidence of stellar halo sub-structure in all four panels. Displaying the density distribution of the BHBs at around the LMC's distance, the top left panel emphasizes the dramatic appearance of the S1 structure. Moving further along the line of sight, the top right panel reveals what might appear like tidal debris loops rising above $Y \sim 20^\circ$. The bottom left panel appears the smoothest and most symmetric of the four. Finally, the bottom right panel, corresponding to BHB distances between 80 and 110 kpc, uncovers an arch of a narrow stream-like structure. Dubbed S4a, following the same nomenclature, its base is at $X = 5^\circ, Y = 15^\circ$ and it is easily traced as far as $X = -18^\circ, Y = 18^\circ$. In fact, the denser and the closest to the LMC part of the stream (around $X \sim 0^\circ$) can also be seen in Figures 6 and 7. Note though, that given the low number of stars contributing to the feature and the growing levels of contamination at these apparent magnitudes, the S4a structure can be a mere chance alignment of BHB candidate stars. If confirmed as a genuine stream, however, S4a can deliver powerful constraints on the properties of the dark matter distribution in the LMC.

The extent of the LMC's stellar halo can be gauged by comparing the distribution of the BHB sub-structure as revealed in each panel of Figure 9 with the reference point at $X = -15^\circ, Y = 25^\circ$ (red filled circle). The 3D separation between the LMC's centre and the reference point is calculated assuming the mean heliocentric distance in each $m - M$ bin. Depending on the distance range considered, the stellar halo sub-structure traced by the BHBs in the DES Year 1 data reaches distances between 25 and 50 kpc away from the LMC's centre.

4.2.2 S2 stream

The S2 stream crosses the DES Year 1 footprint almost vertically along the Dec direction (see Figure 7). The stream's track is well represented with the great circle with the pole at $(\alpha, \delta) = (298.^\circ5, 177^\circ)$. As clear from Figure 6, the stream passes between the two Magellanic Clouds, almost perpendicular to the line connecting the two galaxies, somewhat closer to the SMC. The stream's heliocentric distance is approximately in between the LMC's and the SMC's, at 56 kpc. As can be gleaned from the middle top panel of Figure 8, there is a hint of a positive distance gradient in the trailing direction of the LMC's motion, i.e. decreasing X. Figure 10 gives the view of S2 in the coordinate system aligned with the stream. As demonstrated in the left panel of the Figure, the current DES footprint covers the S2 debris in the range $15^\circ < X_{S2} < 33^\circ$. At the distance of S2, this translates into 15 and 33 kpc away from the line connecting the LMC and the SMC. The right panel of Figure 10 shows the across-stream profile of the S2 debris. As indicated by the overlaid red line, the stream's density can be approximated with a Gaussian profile with FWHM$\sim 3.^\circ5$, or at the S2's distance, ~ 3.5 kpc. Given the fact that the width of the stream is substantial, but seemingly smaller than what is expected

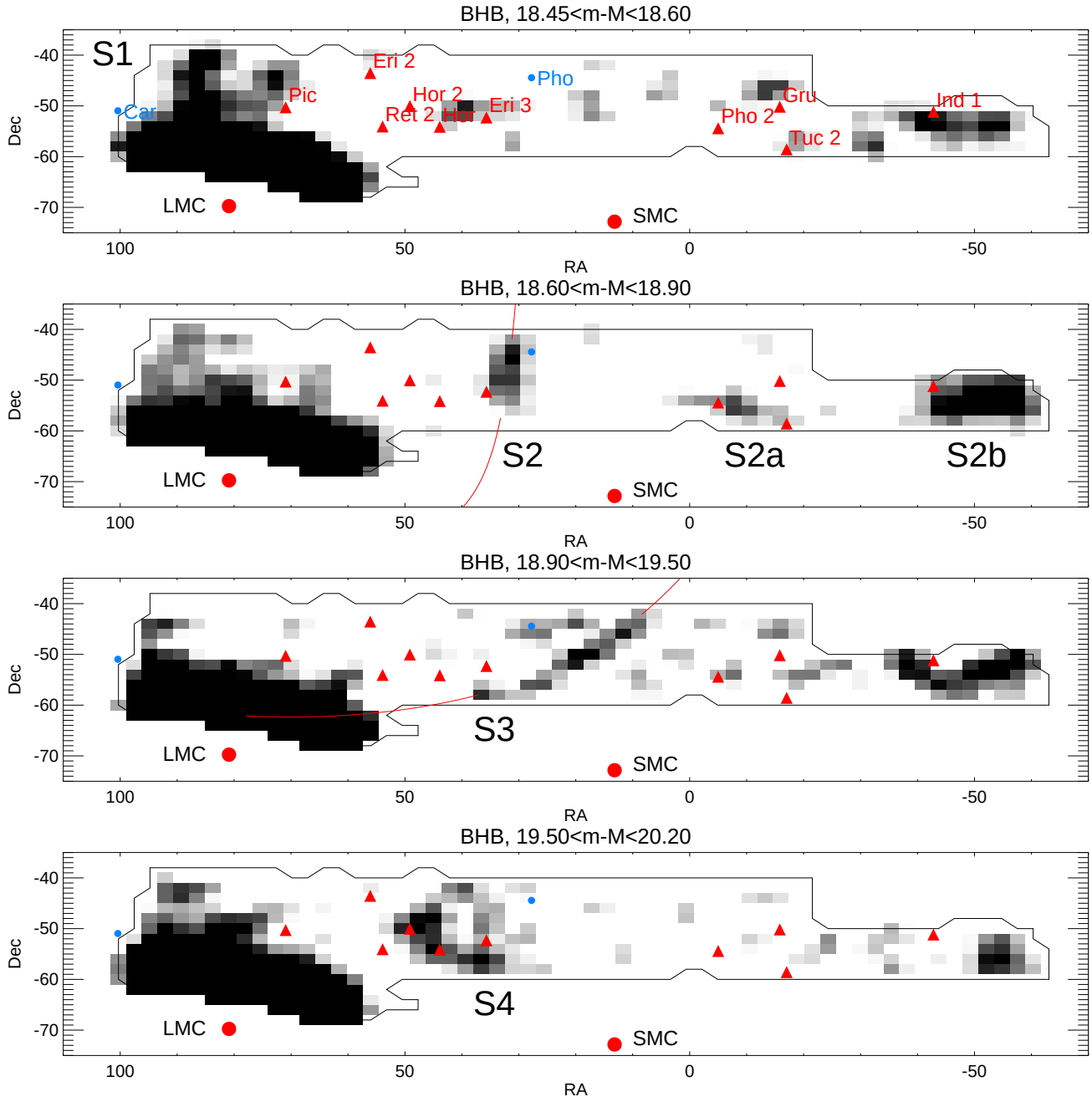

Figure 7. Magellanic stellar streams in equatorial coordinates. Top to bottom: density distributions of the BHB stars selected to lie in the four heliocentric distance bins described earlier. The maps are 60×25 pixels, and are smoothed with a Gaussian kernel with a FWHM of 2 pixels. Red filled circles show the locations of the LMC and the SMC, small blue filled circles mark the positions of the previously known satellites, while the red triangles correspond to the DES Year 1 satellites. Red lines show the great circle for streams S2 and S3. All structures identified in the gnomonic projection in the Figure 6 are also present in these maps. Additionally, three more possible detections are noticeable, i.e. those at RA$\sim -10^\circ$ and RA$\sim -50^\circ$. Given that these structures are most prominent in the distribution of BHBs falling into the 2nd distance bins, they are dubbed S2a and S2b correspondingly. Note that Hor 1, Hor 2 and Eri 3 appear to overlap with the S2 cloud and its counterpart in the 1st distance modulus bin (top panel). Additionally, three other DES Year 1 satellites Pho 2, Gru and Tuc 2 seem to coincide with the S2a cloud.

for the LMC or the SMC, it is perhaps possible the stream originates from a dwarf galaxy disrupting in the tidal field of the Magellanic system. In fact, the aspect ratio of the detected piece of debris is only 5-to-1, therefore rather than a section of a narrow and long stream, S2 could be the remnant of a tidally stretched dwarf galaxy. Note, however, that, if S2 is indeed a stream that orbits one of or both the Magellanic Clouds, it should not, in principle, be aligned with a great circle everywhere on the celestial sphere. Therefore, it is also possible to interpret the S2 debris as a disruption of a system that used to be part of the Magellanic Family in the past and is now orbiting the Milky Way.

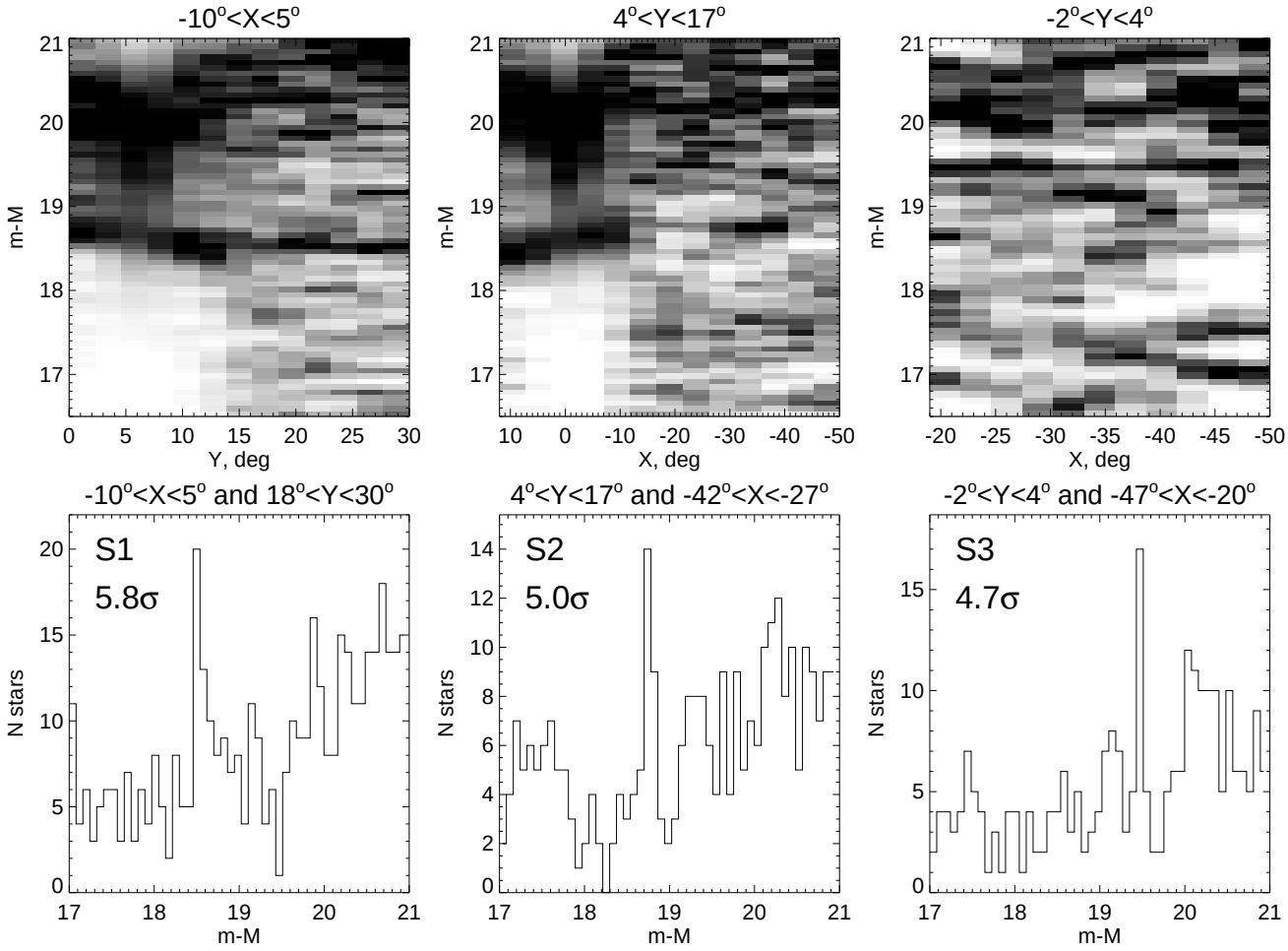

Figure 8. Line-of-sight tomography of structures S1, S2 and S3. *Top:* Density of BHBs in the space of distance modulus and one of the two spatial coordinates (of the gnomonic projection). The density is normalised per column. *Bottom:* Histograms of distance modulus for each of the three structures under consideration. We also give the significance of each structure's peak in the top left corner in every bottom panel. *Left:* This map is 13×70 pixels, and is smoothed with a Gaussian kernel with a FWHM of 1.6 pixels. This is a vertical slice, crossing the LMC's northern regions. The LMC's disk dominates the range $0^\circ < Y < 15^\circ$. A tilt of the disk is clearly visible reflected by a small but perceptible positive distance gradient as a function of Y. Note a narrow, horizontal overdensity connecting to the tilted disk feature around $Y \sim 14^\circ$. This is the S1 debris, located at $m - M \sim 18.5$ and containing in excess of 20 BHBs, as seen in the bottom panel. *Middle:* This map is 13×70 pixels, and is smoothed with a Gaussian kernel with a FWHM of 1.5 pixels. This is a horizontal slice though the LMC. The familiar disk signature is visible at $m - M \sim 18.5$, shadowed by a 'V' shape cloud of the YMS/BS stars. As described in the text, we conjecture that the 'V' shape might be a result of the age gradient across the LMC's disk, with the central parts (at $X \sim 0^\circ$) dominated by the younger (and hence brighter) stellar populations. The S2 stream is visible at $-40^\circ < X < -30^\circ$ and as shown in the bottom panel, its distance modulus distribution peaks around $m - m \sim 18.75$ and contains ~ 20 BHB stars. *Right:* This map is 11×60 pixels, and is smoothed with a Gaussian kernel with a FWHM of 1.7 pixels. Similar to the middle panel, i.e. a horizontal slice, but at lower Y. A very cold feature corresponding to the S3 stream is visible in both the top and the bottom panels. S3 is located at $m - M \sim 19.5$ and contains ∼15 BHB stars.

4.2.3 S3 stream

The S3 stream, running along the great circle with the pole at $(\alpha, \delta) = (250\overset{\circ}{.}15, 152\overset{\circ}{.}35)$, points almost exactly towards the LMC (see Figures 6 and 7). As evidenced by the right column of Figure 8, it is located at the heliocentric distance of ~ 80 kpc, i.e. further away than both of the Magellanic Clouds. Figure 11 presents the view of S3 in the coordinate system aligned with the stream, X_{S3}, Y_{S3}. The apparent width of S3 is clearly quite much smaller as compared to that of S2, as discussed above. The right panel of the Figure shows the across-stream profile, which appears to be only $1\overset{\circ}{.}2$ across, or 1.6 kpc at the distance of the stream. It is not impossible that the stream is actually even narrower than what is indicated by the handful of BHBs detected in the DES data: for example, if the stream's track is not well-described by a great circle, our estimate of the width could be biased high. Given the uncertainty in the stream's width, it is difficult to discern with confidence whether its progenitor was a dwarf galaxy or a globular cluster. As judged by the orientation of its orbit, it might appear to be in the process of being accreted onto the LMC. However, in 3D, the point of its closest approach to the LMC is ~ 20 kpc. If this is indeed the stream's pericentre, it is unlikely that the progenitor could have suffered any significant tidal stripping this far out. Moreover, the caution in the interpretation of the great circle alignment as raised above applies to the S3 stream as well. Overall, the least unlikely scenario seems to be the one in which the stream's progenitor fell into the MW as part of a loose group associated with the LMC. Finally, given the S3's alignment with the Clouds' proper motion and

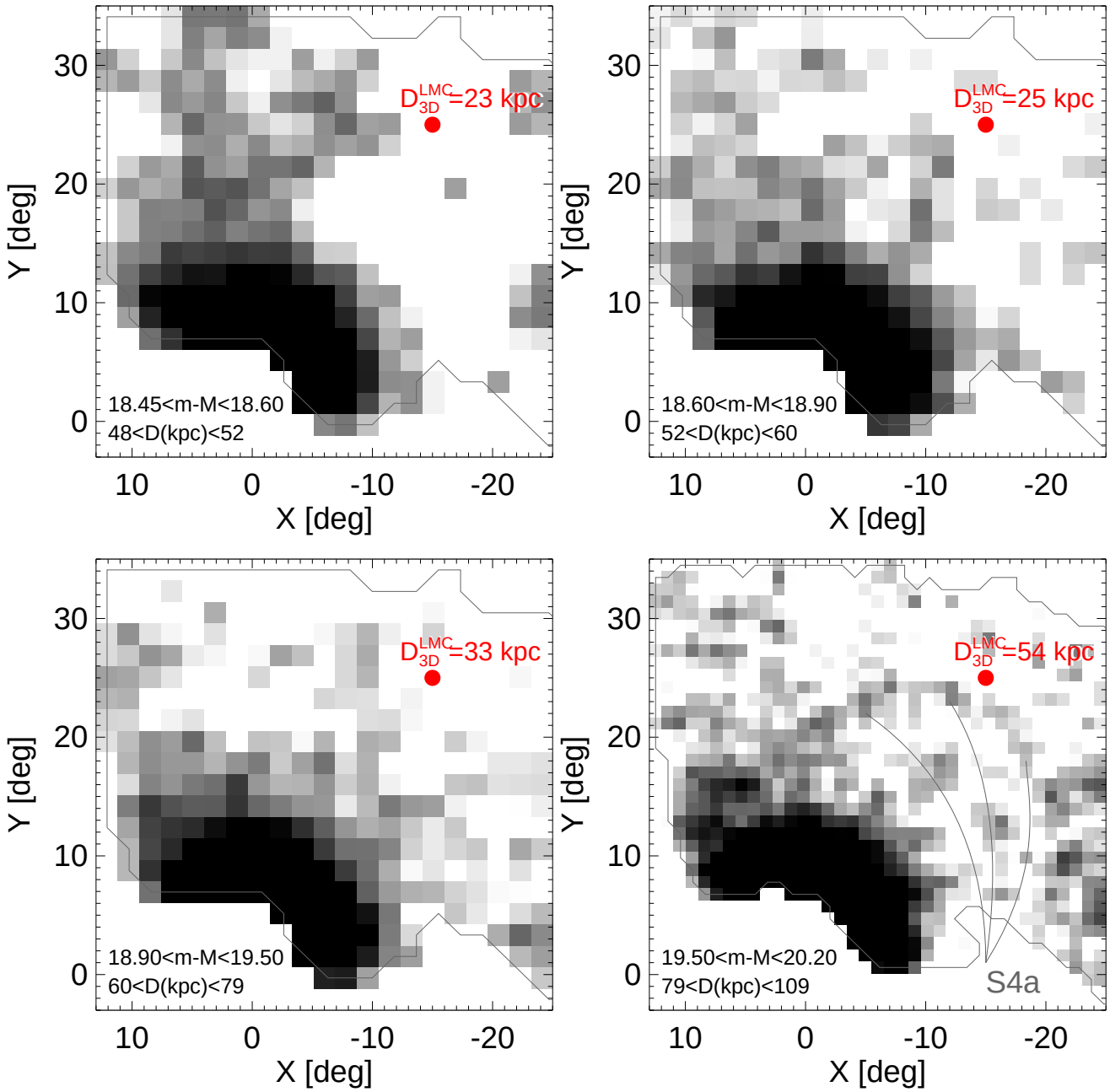

Figure 9. Zoomed-in view of the Northern portion of the LMC stellar halo. Each panel presents the density of BHB selected to have distances in the four distance modulus ranges (given in the bottom left corner). In each case, debris reaching at least $Y = 20^\circ$ are visible. The last panel (bottom right), corresponding the largest $m - M$, also appears to contain a tentative stream-like structure dubbed S4a. Note however, that at this faint magnitudes the background/foreground contamination is most severe. Red filled circle marks the location of a reference point with $X = -15^\circ$ and $Y = 25^\circ$. In each panel, the number next to the red circle gives the 3D distance in kpc of the reference point from the LMC's centre, assuming the mean line-of-sight distance to the debris for each $m - M$ range. The maximal separation between the LMC's centre and the stellar halo sub-structure varies from 25 to 50 kpc.

the overlap with the gaseous MS, it can plausibly be a product of the LMC-SMC interaction.

5 DISCUSSION AND CONCLUSIONS

Most of the previous attempts to find tidally stripped stars at large distances around the Magellanic Clouds have been disappointing as no clear presence of the stellar counterpart to the prominent gaseous stream has been reported. Additionally, only fragmentary glimpses of the alleged LMC's stellar halo have been seen; in fact, many of these detections could be linked directly to the galaxy's disk, rather than the genuine halo. In a bid to produce the final verdict as to the existence of a substantial amount of stellar debris in the halo of the Clouds, we use the deep, wide and continuous coverage of the Magellanic environs provided by the DES Year 1 imaging data. Our tracer of choice is Blue Horizontal Branch stars; to our knowledge, these have not yet been used to study the Clouds. In this

paper, we demonstrate that with the help of the $griz$ photometry, highly complete samples of BHBs can be selected, suffering only moderate levels of contamination from QSOs, WDs and YMS/BS stars. The crucial part in the successful BHB identification is played by the $i-z$ colour, which gauges the flux excess due to differences in the shapes of the Paschen lines in the near-IR part of the spectra of stars with low and high surface gravity. As shown in the top middle panel of Figure 2, the photometric $i-z$ error only starts to blow up at $g \sim 21$, which gives us confidence that thus selected BHBs can trace structures robustly as far as $m-M \sim 20$, i.e. at least 100 kpc.

Armed with a large sample of BHBs detected across several thousands of square degrees, we have exposed – immense in scale and rich in sub-structure – the stellar halo of the Magellanic system. As Figures 4 and 5 demonstrate, around the Clouds, multiple BHB agglomerations exist, stretching from edge to edge of the DES Year 1 footprint, ($\sim 50^\circ$ from the LMC). These sub-structures are clearly dispersed over an enormous volume of tens of kpc: not only they show a complex behaviour as a function of the position on the sky, they also are intertwined along the line of sight, starting from the heliocentric distance of the LMC at $\sim$ 50 kpc and continuing beyond 100 kpc. Note that it is not surprising that we predominantly see stars with distances larger than that of the LMC. This could simply be due to the fact that the DES Year 1 footprint covers the area of the sky predicted to be populated with the trailing (and hence more distant) debris.

If the BHBs are grouped according to their heliocentric distance, overdense regions corresponding to individual stellar streams are immediately obvious. We detect at least four distinct Magellanic stellar halo structures labeled from S1 to S4 according to the distance modulus bin they occupy. An overview of their properties can be found in Figure 6. These discoveries represent the very first census of the Magellanic stellar halo sub-structure. Different in shape, extent and luminosity, each of these clearly, deserves its own detailed analysis, which due to the obvious lack of space, can not be part of this Paper. Nevertheless, a few important highlights are worth mentioning. For example, S1 is the nearest of the structures discovered and is the only one unambiguously connected to the LMC. Even though it stretches to at least $\sim 30^\circ$ from the LMC, its true extent is not known since at its most distant point, the stream is cut-off by the DES Year 1 footprint. As far as we can see, S1 does not appear to be directly related to the 10 kpc stellar stream recently reported by Mackey et al. (2015). Moreover, as evidenced by the top left panel of Figure 8, around the location where S1 decouples from the LMC disk BHB sequence, its debris do not seem to follow the apparent disk's distance gradient (note the discontinuity at $Y \sim 15^\circ$). This might imply a different origin for S1, perhaps in the LMC's stellar halo.

We have also discovered two narrow stellar streams at distances beyond 30° from the LMC. S2 and S3 are also further away along the line of sight, at 56 kpc and 80 kpc correspondingly. The FWHM of S2 is $\sim 3\overset{\circ}{.}5$ and thus it is clearly the product of a disruption of a dwarf galaxy. S3 is even narrower, with FWHM$\sim 1\overset{\circ}{.}2$. However, the stream's width might only be an upper bound as the true trajectory of S3 is unclear. In fact, both S2 and S3, at least their parts visible in the DES Year 1 data, run approximately along great circles. This could be the result of the incomplete view of the streams, to be rectified when more area near the Clouds is available. It is, however, not impossible that S2 and S3 indeed do not curve around either of the galaxies and are now orbiting the Milky Way instead. Interestingly, both S2 and S3 appear to be approximately aligned with the proper motion of the Clouds. Moreover,

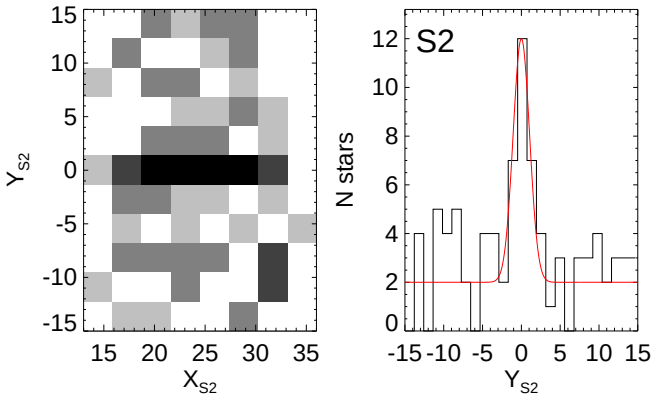

Figure 10. S2 stream. BHBs with distances $18.6 < m-M < 18.9$ are shown in the coordinate system aligned with the stream X_{S2}, Y_{S2}, i.e. with the great circle with the pole at $(\alpha, \delta) = (298\overset{\circ}{.}5, 177^\circ)$. The origin of the X_{S2} axis is the projection of the SMC's position onto the great circle. *Left:* Density of stars in X_{S2}, Y_{S2}. *Right:* Across-stream density profile of the stream as traced by the stars with distances as described above and $15^\circ < X_{S2} < 35^\circ$. To guide the eye, red line shows a Gaussian profile with $\sigma = 1\overset{\circ}{.}5$

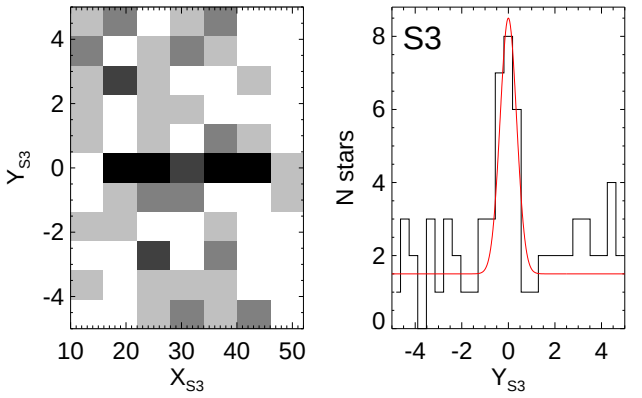

Figure 11. S3 stream. BHBs with distances $19.3 < m-M < 19.6$ are shown in the coordinate system aligned with the stream X_{S3}, Y_{S3}, i.e. with the great circle with the pole at $(\alpha, \delta) = (250\overset{\circ}{.}15, 152\overset{\circ}{.}35)$. The origin of the X_{S3} axis is the projection of the LMC's position onto the great circle. *Left:* Density of stars in X_{S3}, Y_{S3}. *Right:* Across-stream density profile of the stream as traced by the stars with distances as described above and $15^\circ < X_{S3} < 51^\circ$. To guide the eye, red line shows a Gaussian profile with $\sigma = 0\overset{\circ}{.}5$

S3 overlaps with the Magellanic Stream on the sky. Could these therefore be the stellar counterparts of the broader gaseous MS? It is difficult to rule the hypothesis out, given that narrow streams (like S2 and S3) can actually be produced in the disruption of a massive dwarf galaxy, provided the progenitor is not a pressure supported system but a cold rotating disk (see e.g. D'Onghia et al. 2009; Peñarrubia et al. 2010). In fact, both the LMC and the SMC seem to fit the bill.

Amorphous in appearance, the S4 and S2a clouds are more difficult to interpret without the help of a detailed numerical simulation of the Clouds' disruption. It is curious, nonetheless, that several of the recently discovered DES satellites seem to coincide with either of these in both position on the sky and the distance along the line of sight. Figure 9 zooms in onto the regions of the sky between 10° and 30° from the LMC. This is the very first sweeping

panorama of the Cloud's stellar halo. Even in this limited view, it appears gigantic in size: overdensities are detected as far as $\sim 30^\circ$ from the LMC, corresponding to 3D distances from 25 kpc to 50 kpc. We therefore hypothesize that the break in the LMC's stellar density at 13.5 kpc from its centre reported by Balbinot et al. (2015a) is not a sign of the tidal truncation but rather of the transition from the (perturbed) disk to the stellar halo. Note that none of the structures presented here overlap in 3D with the Phoenix stream and the Eridanus-Phoenix cloud recently discovered in the same region of the sky, but at much lower distances by Balbinot et al. (2015b) and Li et al. (2015).

Faced with the wealth and the expanse of the stellar halo substructure discovered, it is prudent to ask whether the LMC could in fact be much more massive than has been assumed until recently. Currently, the mass distribution in the LMC has only been probed out to ∼9 kpc from the dwarf's centre, where according to van der Marel et al. (2002) it adds up to $\sim 9 \times 10^9 M_\odot$. Therefore, many of the numerical MS models assumed a total of $\sim 10^{10} M_\odot$ for the LMC's mass (see e.g. Connors et al. 2006; Diaz & Bekki 2012). However, several new - albeit indirect - clues have been identified that imply that the total mass of the Cloud could be at least an order of magnitude higher. For example, Besla et al. (2012) found that the infall of an LMC with a total mass of $\sim 2 \times 10^{11} M_\odot$ could explain many of the key properties of the Magellanic Stream. On the other hand, a simulation based on low mass LMC appears equally successful (see e.g. Diaz & Bekki 2012). Additionally, Deason et al. (2015) confirmed with a suite of high-resolution Cosmological N-body simulations, that a recent accretion of a massive, i.e. $> 10^{11} M_\odot$ LMC would account for a large number of satellites detected in the DES footprint. Note, however, that according to the earlier study of Sales et al. (2011) even a much smaller mass LMC, i.e. that with $3 \times 10^{10} M_\odot$, could drag an impressive amount of low-mass substructure into the MW halo. Importantly, in light of their relatively high velocities, keeping the Clouds a bound pair for a significant fraction of the Hubble time also requires an LMC with a mass exceeding $10^{11} M_\odot$ (see Kallivayalil et al. 2013). Finally, using an extended timing argument calculation, although not taking the presence of the M33 into account, Peñarrubia et al. (2015) estimated that the LMC's mass could easily be 2.5×10^{11} $M_\odot$.

Notwithstanding the large number of numerical experiments dedicated to the analysis of the Magellanic infall, the only channel of its stellar halo formation that has been explored so far is that due to the LMC-SMC interaction. Most models produce plenty of the SMC stellar spraying around the LMC. However, even in the recent treatise of Besla et al. (2012) and Diaz & Bekki (2012), very little SMC stellar debris can be seen in the area of the sky discussed here, i.e. $Y > 0^\circ$, and almost none at $Y > 15^\circ$. Could any of the stellar sub-structure identified here be due to accretion and tidal disruption of smaller mass satellites? According to the most recent abundance matching projections, some ~ 50 dwarf satellites could have orbited the LMC (see e.g. Deason et al. 2015). The number of star clusters with apo-centres beyond 10 kpc from the Cloud is more difficult to estimate. The question of such high-orbit cluster production is linked to the poorly understood specific frequency of GCs in the dwarf satellites of the LMC. The possibility of cluster formation in the intra-cloud space has not been ruled out either, nor has the exchange of star clusters between the LMC and the SMC. If numerous star clusters and dwarf galaxies did orbit the LMC, it is perhaps possible that a fraction of these could be tidally stripped to produce at least some of the stellar halo observed in the DES data. This, of course, would require favourable orbits, i.e. such that would bring the satellite into the densest regions of the LMC, well within the inner 10 kpc.

What is the orbital history of the Clouds? How did their interaction proceed? What was the satellite luminosity function in the LMC? What is the mass profile of the LMC? These questions can now be addressed through a combination of the deep imaging and spectroscopic follow up of the tidal debris uncovered in this work.

ACKNOWLEDGMENTS

The authors wish to thank Wyn Evans, Mike Irwin, Denis Erkal, Jonathan Diaz and Natalia Mora-Sitjà for illuminating discussions that helped to improve this manuscript. We are grateful to the anonymous referee for the helpful comments they have provided. The research leading to these results has received funding from the European Research Council under the European Union's Seventh Framework Programme (FP/2007-2013) / ERC Grant Agreement n. 308024. V.B. and S.K. acknowledge financial support from the ERC. This research was made possible through the use of the AAVSO Photometric All-Sky Survey (APASS), funded by the Robert Martin Ayers Sciences Fund.

REFERENCES

Ahn, C. P., Alexandroff, R., Allende Prieto, C., et al. 2012, ApJS, 203, 21
Alves, D. R. 2004, ApJ, 601, L151
Amorisco, N. C., Evans, N. W., & van de Ven, G. 2014, Nature, 507, 335
Balbinot, E., Santiago, B. X., Girardi, L., et al. 2015, MNRAS, 449, 1129
Balbinot, E., Yanny, B., Li, T. S., et al. 2015, arXiv:1509.04283
Bell, E. F., Xue, X. X., Rix, H.-W., Ruhland, C., & Hogg, D. W. 2010, AJ, 140, 1850
Belokurov, V. et al. 2006, ApJl, 647, L111
Belokurov, V., Evans, N. W., Irwin, M. J., et al. 2007, ApJ, 658, 337
Belokurov, V., Koposov, S. E., Evans, N. W., et al. 2014, MNRAS, 437, 116
Besla, G., Kallivayalil, N., Hernquist, L., et al. 2007, ApJ, 668, 949
Besla, G., Kallivayalil, N., Hernquist, L., et al. 2010, ApJ, 721, L97
Besla, G., Kallivayalil, N., Hernquist, L., et al. 2012, MNRAS, 421, 2109
Besla, G., Hernquist, L., & Loeb, A. 2013, MNRAS, 428, 2342
Brueck, M. T., & Hawkins, M. R. S. 1983, A&A, 124, 216
Connors, T. W., Kawata, D., & Gibson, B. K. 2006, MNRAS, 371, 108
Davies, R. D., & Wright, A. E. 1977, MNRAS, 180, 71
Deason, A. J., Belokurov, V., & Evans, N. W. 2011, MNRAS, 416, 2903
Deason, A. J., Belokurov, V., Evans, N. W., et al. 2012, MNRAS, 425, 2840
Deason, A. J., Belokurov, V., Koposov, S. E., & Rockosi, C. M. 2014, ApJ, 787, 30
Deason, A. J., Wetzel, A. R., Garrison-Kimmel, S., & Belokurov, V. 2015, MNRAS, 453, 3568
Diaz, J., & Bekki, K. 2011, MNRAS, 413, 2015
Diaz, J. D., & Bekki, K. 2012, ApJ, 750, 36

D'Onghia, E., Besla, G., Cox, T. J., & Hernquist, L. 2009, Nature, 460, 605
Erkal, D. et al, 2015, in prep.
Feast, M. W. 1968, MNRAS, 140, 345
Fermani, F., & Schönrich, R. 2013, MNRAS, 430, 1294
Freeman, K. C., Illingworth, G., & Oemler, A., Jr. 1983, ApJ, 272, 488
Gallart, C., Stetson, P. B., Hardy, E., Pont, F., & Zinn, R. 2004, ApJ, 614, L109
Gardiner, L. T., & Noguchi, M. 1996, MNRAS, 278, 191
Graczyk, D., Pietrzyński, G., Thompson, I. B., et al. 2014, ApJ, 780, 59
Grillmair, C. J., & Dionatos, O. 2006, ApJ, 643, L17
Guhathakurta, P., & Reitzel, D. B. 1998, Galactic Halos, 136, 22
Harris, J., & Zaritsky, D. 2006, AJ, 131, 2514
Heller, P., & Rohlfs, K. 1994, A&A, 291, 743
Irwin, M. J. 1991, The Magellanic Clouds, 148, 453
Johnston, K. V. 1998, ApJ, 495, 297
Kallivayalil, N., van der Marel, R. P., Alcock, C., et al. 2006, ApJ, 638, 772
Kallivayalil, N., van der Marel, R. P., & Alcock, C. 2006, ApJ, 652, 1213
Kallivayalil, N., van der Marel, R. P., Besla, G., Anderson, J., & Alcock, C. 2013, ApJ, 764, 161
Kinman, T. D., Stryker, L. L., Hesser, J. E., et al. 1991, PASP, 103, 1279
Koposov, S. E., Belokurov, V., Evans, N. W., et al. 2012, ApJ, 750, 80
Koposov, S. E., Irwin, M., Belokurov, V., et al. 2014, MNRAS, 442, L85
Koposov, S. E., Belokurov, V., Torrealba, G., & Evans, N. W. 2015, ApJ, 805, 130
Kunkel, W. E., Irwin, M. J., & Demers, S. 1997, A&AS, 122, 463
Li, T. S., Balbinot, E., Mondrik, N., et al. 2015, arXiv:1509.04296
Lin, D. N. C., & Lynden-Bell, D. 1977, MNRAS, 181, 59
Lin, D. N. C., Jones, B. F., & Klemola, A. R. 1995, ApJ, 439, 652
Majewski, S. R., Skrutskie, M. F., Weinberg, M. D., & Ostheimer, J. C. 2003, ApJ, 599, 1082
Mackey, D., Koposov, S. E., Erkal, D., et al. 2015, arXiv:1508.01356
Majewski, S. R., Ostheimer, J. C., Kunkel, W. E., et al. 1999, New Views of the Magellanic Clouds, 190, 508
Majewski, S. R., Nidever, D. L., Muñoz, R. R., et al. 2009, IAU Symposium, 256, 51
Martínez-Delgado, D., Romanowsky, A. J., Gabany, R. J., et al. 2012, ApJ, 748, L24
Mastropietro, C., Moore, B., Mayer, L., Wadsley, J., & Stadel, J. 2005, MNRAS, 363, 509
Mathewson, D. S., Cleary, M. N., & Murray, J. D. 1974, ApJ, 190, 291
McConnachie, A. W. 2012, AJ, 144, 4
McMahon, R., & Irwin, M. 1989, GEMINI Newsletter Royal Greenwich Observatory, 25, 6
McMonigal, B., Bate, N. F., Lewis, G. F., et al. 2014, MNRAS, 444, 3139
Meurer, G. R., Bicknell, G. V., & Gingold, R. A. 1985, Proceedings of the Astronomical Society of Australia, 6, 195
Minniti, D., Borissova, J., Rejkuba, M., et al. 2003, Science, 301, 1508
Moore, B., & Davis, M. 1994, MNRAS, 270, 209
Muñoz, R. R., Majewski, S. R., Zaggia, S., et al. 2006, ApJ, 649, 201
Murai, T., & Fujimoto, M. 1980, PASJ, 32, 581
Nidever, D. L., Majewski, S. R., & Burton, W. B. 2008, ApJ, 679, 432
Nidever, D. L., Majewski, S. R., Butler Burton, W., & Nigra, L. 2010, ApJ, 723, 1618
Nidever, D. L., Majewski, S. R., Muñoz, R. R., et al. 2011, ApJ, 733, L10
Newberg, H. J., Yanny, B., Grebel, E. K., et al. 2003, ApJ, 596, L191
Odenkirchen, M., Grebel, E. K., Dehnen, W., et al. 2003, AJ, 126, 2385
Olszewski, E. W., Suntzeff, N. B., & Mateo, M. 1996, ARA&A, 34, 511
Pejcha, O., & Stanek, K. Z. 2009, ApJ, 704, 1730
Peñarrubia, J., Belokurov, V., Evans, N. W., et al. 2010, MNRAS, 408, L26
Peñarrubia, J., Gómez, F. A., Besla, G., Erkal, D., & Ma, Y.-Z. 2015, arXiv:1507.03594
Pietrzyński, G., Graczyk, D., Gieren, W., et al. 2013, Nature, 495, 76
Putman, M. E., Staveley-Smith, L., Freeman, K. C., Gibson, B. K., & Barnes, D. G. 2003, ApJ, 586, 170
Schönrich, R., Binney, J., & Dehnen, W. 2010, MNRAS, 403, 1829
Recillas-Cruz, E. 1982, MNRAS, 201, 473
Ruhland, C., Bell, E. F., Rix, H.-W., & Xue, X.-X. 2011, ApJ, 731, 119
Rich, R. M., Collins, M. L. M., Black, C. M., et al. 2012, Nature, 482, 192
Saha, A., Olszewski, E. W., Brondel, B., et al. 2010, AJ, 140, 1719
Sales, L. V., Navarro, J. F., Cooper, A. P., et al. 2011, MNRAS, 418, 648
Sanduleak, N. 1980, PASP, 92, 246
Schlegel, D. J., Finkbeiner, D. P., & Davis, M. 1998, ApJ, 500, 525
Schlafly, E. F., & Finkbeiner, D. P. 2011, ApJ, 737, 103
Shanks, T., Metcalfe, N., Chehade, B., et al. 2015, MNRAS, 451, 4238
Sirko, E., Goodman, J., Knapp, G. R., et al. 2004, AJ, 127, 899
van der Marel, R. P., Alves, D. R., Hardy, E., & Suntzeff, N. B. 2002, AJ, 124, 2639
van der Marel, R. P., & Kallivayalil, N. 2014, ApJ, 781, 121
Vickers, J. J., Grebel, E. K., & Huxor, A. P. 2012, AJ, 143, 86
Wannier, P., & Wrixon, G. T. 1972, ApJ, 173, L119
Weinberg, M. D. 2000, ApJ, 532, 922
Xue, X. X., Rix, H. W., Zhao, G., et al. 2008, ApJ, 684, 1143
Yanny, B., et al. 2000, ApJ, 540, 825